

CCUTH-96-03
NHCU-HEP-96-15

Three-Scale Factorization Theorem and Effective Field Theory

Chia-Hung V. Chang¹ and Hsiang-nan Li²

¹Department of Physics, National Tsing-Hua University,
Hsin-Chu, Taiwan, R.O.C.

²Department of Physics, National Chung-Cheng University,
Chia-Yi, Taiwan, R.O.C.

February 1, 2008

Abstract

We develop a perturbative QCD factorization theorem which is compatible with effective field theory. The factorization involves three scales: an infrared cutoff of order Λ_{QCD} , a hard scale of order the B meson mass, and an ultraviolet cutoff of order the W boson mass. Our approach is renormalization group invariant and moderates the scale-dependence problem in effective field theory. Applying this formalism to exclusive nonleptonic B meson decays, we clarify the controversy over the Bauer-Stech-Wirbel parameters a_2/a_1 for charm and bottom decays. It is found that the nonfactorizable contribution plays an important role in the explanation of the sign and magnitude of a_2/a_1 .

Nonleptonic heavy meson decays are difficult to analyze due to the complicated QCD corrections. While the semileptonic decays involve only conserved currents, the nonleptonic decays are described by four-quark current-current operators, which is part of the low-energy effective Hamiltonians for the W boson exchange. For example, the relevant operator for the $B \rightarrow D\pi$ decays is

$$H = \frac{4G_F}{\sqrt{2}} V_{cb} V_{ud}^* (\bar{c}_L \gamma_\mu b_L) (\bar{d}_L \gamma^\mu u_L) , \quad (1)$$

The QCD corrections will generate operator mixing among these operators. The mixing, characterized by Wilson coefficients, depends on an arbitrary renormalization scale μ . The full effective Hamiltonian related to Eq. (1) can be written as

$$H_{\text{eff}} = \frac{4G_F}{\sqrt{2}} V_{cb} V_{ud}^* [c_1(\mu) O_1 + c_2(\mu) O_2] , \quad (2)$$

with

$$O_1 = (\bar{c}_L \gamma_\mu b_L) (\bar{d}_L \gamma^\mu u_L) , \quad O_2 = (\bar{d}_L \gamma_\mu b_L) (\bar{c}_L \gamma^\mu u_L) . \quad (3)$$

In Eq. (2) c_1 and c_2 are the Wilson coefficients, whose evolution from the W boson mass M_W down to a lower scale is determined by renormalization-group running [1]. Though the Wilson coefficients are μ dependent, physical quantities such as decay amplitudes are not. In principle, the matrix elements of the four-fermion operators contain a μ dependence, which exactly cancels that of the Wilson coefficients. In practical applications, however, various schemes are needed to estimate the hadronic matrix elements, and the estimates are usually μ independent. Hence, the decay amplitudes turn out to be scale dependent. Take exclusive nonleptonic B meson decays as an example, to which the conventional approach is the Bauer-Stech-Wirbel (BSW) factorization approximation [2]. It is assumed that nonleptonic matrix elements can be factorized into two matrix elements of (axial) vector currents. Since the currents are conserved, the matrix elements have no anomalous scale dependence. Presumably μ should be set to the dominant scale of the matrix

elements. However, the matrix elements involve both the heavy quark scale and the small hadronic scale. Naively setting μ to the heavy quark mass will lose large logarithms associated with the hadronic scale. It is then quite natural that theoretical predictions are sensitive to the scale we choose [3, 4].

To circumvent this problem, a phenomenological approach is adopted to bypass the strong scale dependence. The Wilson coefficients c_i are regarded as free parameters, and are determined by experimental data [2]. In this model, two equivalent parameters $a_1 = c_1 + c_2/N_c$ and $a_2 = c_2 + c_1/N_c$ describe the external and internal W -emission amplitudes, respectively. However, the evaluation of the hadronic form factors usually involve some ansatz [5] and thus the extraction of a_1 and a_2 is model dependent. It is also found that only when the experimental errors are expanded greatly does an allowed domain (a_1, a_2) exist for the three classes of decays $\bar{B}^0 \rightarrow D^{(*)+}$, $\bar{B}^0 \rightarrow D^{(*)0}$ and $B^- \rightarrow D^{(*)0}$ [6]. In addition, a negative a_2/a_1 and a positive a_2/a_1 are concluded from the data of charm and bottom decays [2, 7], respectively.

It was shown recently that the perturbative QCD (PQCD) approach is applicable to heavy meson decays [8, 9], to which the heavy mass provides the large momentum transfer. The breakthrough is due to the all-order Sudakov resummation of large radiative corrections, which suppress contributions from the long-distance region. This formalism, taking into account the evolution from the typical scale of the hard subprocesses characterized by the heavy meson mass to a lower hadronic scale, is μ independent for semileptonic decays. In this letter we shall develop a PQCD formalism based on the effective Hamiltonian in Eq. (2), which further incorporates the evolution from M_W down to the hard scale. This three-scale factorization theorem, being μ independent, does not suffer the scale-setting ambiguity mentioned above. We apply this formalism to two-body nonleptonic B meson decays such as $B \rightarrow D\pi$. Without any free parameter, our prediction agrees well with experimental data.

We first illustrate the main idea of PQCD factorization theorems by con-

sidering one-loop QCD corrections to a generic decay process through a current. These corrections are ultraviolet finite, since the conserved current is not renormalized. However, they also give rise to infrared divergences, when the gluons are soft or collinear to light partons. The factorization is implemented to isolate these infrared divergences associated with the long-distance physics.

Radiative corrections that produce infrared divergences are classified into the reducible and irreducible types [10]. Irreducible corrections contain only single soft logarithms and is absorbed into a soft function U , which corresponds to the nonfactorizable soft corrections in B meson decays in the literature [5]. These corrections cancel asymptotically [10], and thus are expected to be small. They will be neglected here (*ie* $U = 1$) and studied in a forthcoming work. Reducible corrections contain double logarithms from the combination of soft and collinear divergences, which can be absorbed into a wave function $\phi(P, b, \mu)$ and explicitly resummed into a Sudakov factor [10],

$$\phi(P, b, \mu) = \exp[-s(P, b)]\phi(b, \mu) . \quad (4)$$

b is the conjugate variable of the transverse momentum, which will be explained later, and $1/b$ can be regarded as an infrared cutoff.

To factorize a one-loop correction, we divide it into two terms as shown in Fig. 1(a). The first term, with eikonal approximation for fermion propagators, picks up the infrared structure of the full diagram. Being infrared sensitive, it is absorbed into U or ϕ , depending on which type the one-loop correction is. The second term, with a soft subtraction, is infrared safe. It has the same ultraviolet structure as the full diagram and can be absorbed into a hard scattering amplitude $H(t, \mu)$, where t denotes the typical scale of the hard decay process. We then get the $O(\alpha_s)$ factorization formula shown in Fig. 1(b), where the diagrams in the first parentheses contribute to H .

The presence of μ implies that both ϕ and H need renormalization. Let γ_ϕ be the anomalous dimension of ϕ . Then the anomalous dimension of H must

be $-\gamma_\phi$, because the full diagram does not contain ultraviolet divergences. Their μ dependence can be calculated by RG,

$$\phi(b, \mu) = \phi(b, 1/b) \exp \left[- \int_{1/b}^{\mu} \frac{d\bar{\mu}}{\bar{\mu}} \gamma_\phi(\alpha_s(\bar{\mu})) \right], \quad (5)$$

$$H(t, \mu) = H(t, t) \exp \left[- \int_{\mu}^t \frac{d\bar{\mu}}{\bar{\mu}} \gamma_\phi(\alpha_s(\bar{\mu})) \right]. \quad (6)$$

Equation (5) describes the evolution of ϕ from $1/b$ to an arbitrary scale μ , and (6) describes the evolution of H from μ to t . The contribution characterized by momenta smaller than $1/b$, *ie.*, the infrared divergence, is absorbed into the initial condition $\phi(b, 1/b)$, which is of nonperturbative origin. The convolution of H with ϕ is then μ independent as indicated by

$$H(t, \mu) \phi(b, \mu) = H(t, t) \phi(b, 1/b) \exp \left[- \int_{1/b}^t \frac{d\bar{\mu}}{\bar{\mu}} \gamma_\phi(\alpha_s(\bar{\mu})) \right]. \quad (7)$$

In this way all the large single logarithms are collected in the exponential.

Indeed the effective Hamiltonian in Eq. (2) can be constructed in a similar way. Consider now a typical one-loop QCD correction to the W boson exchange diagram Fig. 1(c). We express the full diagram, which is ultraviolet finite, into two terms as shown in Fig. 1(c). The first term, obtained by shrinking the W boson line into a vertex, corresponds to the local four-fermion operators O_i . It is absorbed into a hard scattering amplitude $H(t, \mu)$, with a typical scale $t \ll M_W$, since gluons involved in this term do not “see” the W boson. Its dependence on M_W is limited to the $1/M_W^2$ factor of the four-fermion operators. The second term, characterized by momenta of order M_W , is absorbed into a “harder” function $H_r(M_W, \mu)$ (not a scattering amplitude), in which gluons do “see” the W boson.

We obtain the $O(\alpha_s)$ factorization formula shown in Fig. 1(d), where the diagrams in the first parentheses contribute to H_r , and those in the second parentheses to H . Note that this formula in fact represents a matrix relation because of the mixing between operators O_1 and O_2 . Solving their

RG equations, we derive

$$H_r(M_W, \mu)H(t, \mu) = H_r(M_W, M_W)H(t, t) \exp \left[\int_t^{M_W} \frac{d\bar{\mu}}{\bar{\mu}} \gamma_{H_r}(\alpha_s(\bar{\mu})) \right], \quad (8)$$

where the anomalous dimension γ_{H_r} of H_r is also a matrix. We emphasize that the factorization in Eq. (8) is not complete because of the presence of infrared divergences in H . The exponential can be easily identified as the Wilson coefficient, implying that μ in $c(\mu)$ should be set to the hard scale t . Without large logarithms, $H_r(M_W, M_W)$ can now be safely approximated by its lowest-order expression $H_r^{(0)} = 1$.

We are now ready to construct a three-scale factorization theorem by combining Eqs. (7) and (8). Consider the decay amplitude up to $O(\alpha_s)$ without integrating out the W boson. We first factorize out the infrared sensitive wave functions as described above. Though devoid of infrared divergences (the nonfactorizable soft corrections have been neglected here), the hard part still involves two scales t and M_W . The factorization in Fig. 1(d) is then employed to separate these two scales, and H_r can be moved out of the hard part, a step valid up to $O(\alpha_s)$. We identify the remaining diagrams, including the four-fermion amplitude and the associated soft subtraction, as the hard scattering amplitude H , since it is free of infrared divergences. The anomalous dimension of H is given by $\gamma_H = -(\gamma_\phi + \gamma_{H_r})$. We thus get the three-scale factorization formula

$$H_r(M_W, \mu)H(t, \mu)\phi(b, \mu) = c(t)H(t, t)\phi(b, 1/b) \exp \left[- \int_{1/b}^t \frac{d\bar{\mu}}{\bar{\mu}} \gamma_\phi(\alpha_s(\bar{\mu})) \right], \quad (9)$$

with the Wilson coefficient $c(t)$ given by the exponential factor in Eq. (8). The two-stage evolutions from $1/b$ to t and from t to M_W are both included, and the final expression is μ independent.

The above conclusion is quite natural from the effective field theory approach [11]. An effective field theory is constructed for a scale $\mu < M_W$ by integrating out the W boson at $\mu = M_W$. Matching corrections are determined by the matching condition requiring that the low-energy light-particle

Green functions of the two theories be equal. The effective theory is then evolved by RG running from $\mu = M_W$ to a lower scale, which insures that the amplitudes are μ independent. The scale μ in a continuum effective field theory is actually a scale to separate the long-distance from the short-distance physics with the physics above the scale μ absorbed into the coefficients in the effective Hamiltonian, such as the Wilson coefficients $c_{1,2}(\mu)$. This idea is identical to the PQCD factorization theorem. The effective field theory constructed this way has exactly the same low-energy behaviour as the full theory, including infrared divergences, physical cuts, and etc. Thus the infrared divergences in the decay amplitudes calculated using the effective field theory can be factorized in the same way as the full theory. The factorization formula for the μ independent amplitude is identical to Eq. (9),

$$c(M_W, \mu) H(t, \mu) \phi(b, \mu) , \quad (10)$$

with the Wilson coefficient c identified as H_r .

We now apply the above formalism to the nonleptonic decays $B(P_1) \rightarrow D(P_2) \pi(P_3)$. The decay rate can be written as

$$\Gamma = \frac{1}{128\pi} G_F^2 |V_{cb}|^2 |V_{ud}|^2 M_B^3 \frac{(1-r^2)^3}{r} |\mathcal{M}|^2 , \quad (11)$$

with $r = M_D/M_B$, M_B (M_D) being the B (D) meson mass. In the rest frame of the B meson, P_1 has the components $P_1 = (M_B/\sqrt{2})(1, 1, \mathbf{0}_T)$. The nonvanishing components of P_2 and P_3 are respectively $P_2^+ = M_B/\sqrt{2}$, $P_2^- = rM_D/\sqrt{2}$, $P_3^+ = 0$, and $P_3^- = (1-r^2)M_B/\sqrt{2}$. Let $k_1(k_2)$ be the momentum of the light valence quark in the B (D) meson and k_3 be the momentum of a valence quark in the pion. These k 's may be off-shell by the amount of their transverse components k_T of order Λ_{QCD} . We define the momentum fractions x as $x_1 = k_1^-/P_1^-$, $x_2 = k_2^+/P_2^+$, and $x_3 = k_3^-/P_3^-$. The transverse momenta k_{iT} play the role of an infrared cutoff in our analysis.

To leading power in $1/M_B$, the factorization formula for \mathcal{M} in the trans-

verse configuration space [10] is written as

$$\begin{aligned} \mathcal{M} = & \int_0^1 [dx] \int_0^\infty [d^2\mathbf{b}] \phi_B(x_1, b_1, 1/b_1) \phi_D(x_2, b_2, 1/b_2) \phi_\pi(x_3, b_3, 1/b_3) \\ & \times c(t) H(x_i, b_i, t) \exp[-S(x_i, b_i)] \end{aligned} \quad (12)$$

with $[dx] = dx_1 dx_2 dx_3$ and $[d^2\mathbf{b}] = d^2\mathbf{b}_1 d^2\mathbf{b}_2 d^2\mathbf{b}_3$. The Sudakov factor e^{-S} is the product of e^{-s} in Eq. (4) and the exponential in Eq. (9) from each wave function. In the analysis below we shall neglect the b dependence of the wave functions [8].

Without large logarithms, the hard part H can be reliably treated by perturbation theory. To leading order in α_s , the hard part for the decay $B^- \rightarrow D^0 \pi^-$ consists of four sets of diagrams shown in Fig. 2. The diagrams in Fig. 2(a) correspond to the external W emission [2, 3], while those in Fig. 2(b) to the internal W emission. They have been calculated using the PQCD formalism in [8, 9] without including the Wilson coefficients. Denote their contributions to the amplitude \mathcal{M} as \mathcal{M}_a and \mathcal{M}_b . It is easy to find that the Wilson coefficients associated with \mathcal{M}_a and \mathcal{M}_b are respectively a_1 and a_2 . Readers are referred to [9] for the complete formulas of \mathcal{M}_a and \mathcal{M}_b .

Diagrams in Fig. 2(c) and 2(d) are absent in the factorization approximation and will be called the nonfactorizable diagrams. Fig. 2(c) leads to the amplitude \mathcal{M}_c

$$\begin{aligned} \mathcal{M}_c = & 32\sqrt{2N_c}\pi\mathcal{C}_F\sqrt{r}M_B^2G_F \int_0^1 [dx] \int_0^\infty b_1 db_1 b_2 db_2 \phi_B(x_1) \phi_D(x_2) \phi_\pi(x_3) \\ & \times \left[\alpha_s(t_1) \frac{c_1(t_1)}{N_c} e^{-S_{c1}(x_i, b_i)} (x_1 - x_2 - x_3(1 - r^2)) h_c^{(1)}(x_i, b_i) \right. \\ & \left. + \alpha_s(t_2) \frac{c_1(t_2)}{N_c} e^{-S_{c2}(x_i, b_i)} (1 - (x_1 + x_2)(1 - r^2)) h_c^{(2)}(x_i, b_i) \right]. \end{aligned} \quad (13)$$

The functions $h_c^{(j)}$, $j = 1$ and 2 , are given by

$$\begin{aligned} h_c^{(j)} = & [\theta(b_1 - b_2) K_0(AM_B b_1) I_0(AM_B b_2) + \theta(b_2 - b_1) K_0(AM_B b_2) I_0(AM_B b_1)] \\ & \times \begin{pmatrix} K_0(B_j M_B b_2) & \text{for } B_j \geq 0 \\ \frac{i\pi}{2} H_0^{(1)}(|B_j| M_B b_2) & \text{for } B_j \leq 0 \end{pmatrix}, \end{aligned} \quad (14)$$

with $A^2 = x_1 x_3 (1 - r^2)$, $B_1^2 = (x_1 + x_2) r^2 - (1 - x_1 - x_2) x_3 (1 - r^2)$, and $B_2^2 = (x_1 - x_2) x_3 (1 - r^2)$. The Sudakov exponent S_{cj} is written as

$$S_{cj} = s(x_1 P_1^+, b_1) + s(x_2 P_2^+, b_2) + s((1 - x_2) P_2^+, b_2) + s(x_3 P_3^-, b_3) \\ + s((1 - x_3) P_3^-, b_3) - \frac{1}{\beta_1} \sum_{i=1}^3 \ln \frac{\ln(t_j/\Lambda)}{-\ln(b_i \Lambda)}, \quad (15)$$

with $b_3 = b_2$, $\beta_1 = (33 - 2n_f)/12$ and $n_f = 4$ the number of flavors. The scale t_j is chosen as $t_j = \max(AM_B, |B_j|M_B, 1/b_1, 1/b_2)$, and $\Lambda \equiv \Lambda_{\text{QCD}}$ is set to 0.2 GeV. The Sudakov suppression described by the factor $\exp(-S_c)$ then warrants that main contributions come from the small b , or large t , region, in which $\alpha_s(t)$ is small, and thus the perturbative treatment of the hard part is reliable. The amplitude \mathcal{M}_d is obtained from Fig. 2(d) accordingly. The amplitudes for the decay $\bar{B}^0 \rightarrow D^+ \pi^-$ can be derived in a similar way. However, it is found that only the external W -emission contribution, the same as \mathcal{M}_a , is important. Therefore, we shall not give its expression here.

The wave functions are chosen as [9],

$$\phi_\pi(x) = \frac{5\sqrt{6}}{2} f_\pi x(1-x)(1-2x)^2, \quad \phi_{B,D}(x) = \frac{N_{B,D}}{16\pi^2} \frac{x(1-x)^2}{M_{B,D}^2 + C_{B,D}(1-x)}, \quad (16)$$

where $f_\pi = 132$ MeV is the pion decay constant. $N_B = 650.212$ and $C_B = -27.1051$ correspond to the B meson decay constant $f_B = 200$ MeV. N_D is determined by the D meson decay constant $f_D = 220$ MeV, and C_D is fixed by data for the decay $\bar{B}^0 \rightarrow D^+ \pi^-$ [9]. All other parameters are referred to [9].

The experimental data of the branching ratios are $\mathcal{B}_0 = \mathcal{B}(\bar{B}^0 \rightarrow D^+ \pi^-) = (3.08 \pm 0.85) \times 10^{-3}$ and $\mathcal{B}_- = \mathcal{B}(B^- \rightarrow D^0 \pi^-) = (5.34 \pm 1.05) \times 10^{-3}$ [12]. Our predictions using the original Hamiltonian in Eq. (1), *ie* $c_1 = 1$ and $c_2 = 0$, are $\mathcal{B}_0 = 3.08 \times 10^{-3}$ and $\mathcal{B}_- = 5.10 \times 10^{-3}$. If the three-scale factorization formulas based on the effective Hamiltonian is employed, we obtain $\mathcal{B}_0 = 3.08 \times 10^{-3}$ and $\mathcal{B}_- = 5.00 \times 10^{-3}$, which differ from the previous results

only by 2%. The slight variation justifies the analysis of exclusive nonleptonic B meson decays performed in [9] using Eq. (1). A careful observation reveals that when the evolution of the Wilson coefficients is taken into account, the amplitude \mathcal{M}_b , which is proportional to $a_2(t)$, becomes smaller, while \mathcal{M}_c , which is proportional to $c_1(t)/N_c$, becomes larger. Hence, the two changes cancel each other, and the total decay rate remains almost the same. \mathcal{M}_d is less important because of the pair cancellation between the two diagrams in Fig. 2(d). Our calculation also indicates that the nonfactorizable contribution \mathcal{M}_c is substantial, and the limit of the BSW factorization approximation. That is why the naive choice of $a_{1,2} = a_{1,2}(M_B)$ in the BSW model fails to explain the data.

Applying the three-scale factorization theorem to the mode $D^- \rightarrow K^0 \pi^-$, we obtain the predictions $\mathcal{B}(\bar{D}^0 \rightarrow K^+ \pi^-) = 4.05\%$ and $\mathcal{B}(D^- \rightarrow K^0 \pi^-) = 2.67\%$, consistent with the data $(4.01 \pm 0.14)\%$ and $(2.74 \pm 0.29)\%$, respectively. With the running scale t reaching below the c quark mass, \mathcal{M}_b becomes more negative and overcomes the positive contribution of \mathcal{M}_c . This explains the observed destructive interference of the external and internal W -meson emission contributions absent in the B meson decays. Hence, the nonfactorizable diagrams play an important role in the explanation of the charm decay data. It is clear that a PQCD formalism based on the original Hamiltonian without Wilson coefficients [9, 13] can not account for this change of sign in the charm decays. From the above analysis, we suggest that $c_{1,2}$ could be regarded as Wilson coefficients as they originally are, if the scale is chosen properly, instead of as fitting parameters in the BSW model. That is, the controversy over the extraction of a_2/a_1 from the bottom and charm decays does not exist in our theory.

The scale dependence of our formalism can be tested by substituting $2t$ for t in the factorization formula. It is found that the prediction decreases by only 5%. In the conventional effective field theory, the substitution of M_b by $2M_b$ for the argument of the Wilson coefficients $c_{1,2}$ results in a 10% to

20% difference [4]. Hence, the scale-setting ambiguity is moderated in the three-scale factorization theorems. In conclusion, our formalism provides a more sophisticated choice of the scale, which takes into account the additional low-energy dynamics in the mesons. This approach is expected to give more definitive predictions, when it is applied to inclusive nonleptonic B meson decays. This subject will be discussed elsewhere.

Our formalism can also be applied to the decays $B \rightarrow J/\Psi K^{(*)}$. With the three-scale factorization formulas and the inclusion of nonfactorizable contributions, both the decay rates and the fraction of the longitudinal mode can be explained. The details will be published in a separate work.

This work was supported by the National Science Council of ROC under Grant No. NSC-85-2112-M-194-009 (for H. L.) and NSC-85-2112-M007-029, NSC-85-2112-M007-032 (for C. C.).

References

- [1] G. Buchalla, A. Buras and M. Lautenbacher, hep-ph/9512380.
- [2] M. Bauer, B. Stech and M. Wirbel, Z. Phys. C29, 637 (1985); 34, 103 (1987).
- [3] M. Neubert, V. Rieckert, B. Stech and Q.P. Xu in *Heavy Flavours* ed. by A.J. Buras and M. Lindner.
- [4] M. Luke, M.J. Savage, and M.B. Wise, Phys. Lett. B343, 329 (1995); 345, 301 (1995); E. Bagan, P. Ball, B. Fiol, and P. Gosdzinsky, Phys. Lett. B351, 546 (1995).
- [5] H.Y. Cheng and B. Tseng, Phys. Rev. D51, 6259 (1995).
- [6] M. Gourdin, A.N. Kamal, Y.Y. Keum, and X.Y. Pham, Phys. Lett. B333, 507 (1994).
- [7] A.N. Kamal and T.N. Pham, Phys. Rev. D50, 395 (1994).
- [8] H.-n. Li, Phys. Rev. D52, 3958 (1995); C.Y. Wu, T.W. Yeh, and H.-n. Li, Phys. Rev. D53, 4982 (1996).
- [9] C.Y. Wu, T.W. Yeh, and H.-n. Li, CCUTH-96-01 (hep-ph/9603250).
- [10] H.-n. Li and G. Sterman Nucl. Phys. B381, 129 (1992).
- [11] See, for example, H. Georgi, Ann. Rev. Nucl. Part. Sci, 43, 209 (1993).
- [12] J.L. Rodriguez, hep-ex/9604011; CLEO Collaboration, M.S. Alam *et al.*, Phys. Rev. D50, 43 (1994).
- [13] C.E. Carlson and J. Milana, Phys. Rev. D49, 5908 (1994).

Figure Captions

Fig. 1. (a) Separation of infrared and hard $O(\alpha_s)$ contributions in PQCD. (b) $O(\alpha_s)$ factorization into a wave function and a hard scattering amplitude. (c) Separation of hard and harder $O(\alpha_s)$ contributions in an effective field theory. (d) $O(\alpha_s)$ factorization into a “harder” function and a hard scattering amplitude.

Fig. 2. (a) External W emission. (b) Internal W emission. (c) and (d) Nonfactorizable internal W emission.

$$\begin{array}{c}
\text{Diagram 1} = \text{Diagram 2} + \left(\text{Diagram 3} - \text{Diagram 4} \right) \\
\text{(a)}
\end{array}$$

Diagram 1: A vertical oval between two horizontal lines. A wavy line enters from the bottom left, goes up and around the oval, and exits at the top right. The top end of the wavy line is double-lined.

Diagram 2: Similar to Diagram 1, but the wavy line enters from the bottom left, goes up and around the oval, and exits at the top right. The bottom end of the wavy line is double-lined.

Diagram 3: Similar to Diagram 1, but the wavy line enters from the bottom left, goes up and around the oval, and exits at the top right. The top end of the wavy line is double-lined.

Diagram 4: Similar to Diagram 1, but the wavy line enters from the bottom left, goes up and around the oval, and exits at the top right. The bottom end of the wavy line is double-lined.

$$\left(\text{Diagram 5} + \text{Diagram 6} - \text{Diagram 7} \right) \otimes \left(1 + \text{Diagram 8} \right)$$

Diagram 5: A vertical oval between two horizontal lines.

Diagram 6: Similar to Diagram 1, but the wavy line enters from the bottom left, goes up and around the oval, and exits at the top right. The top end of the wavy line is double-lined.

Diagram 7: Similar to Diagram 1, but the wavy line enters from the bottom left, goes up and around the oval, and exits at the top right. The bottom end of the wavy line is double-lined.

Diagram 8: A wavy line entering from the bottom left, going up and around, and exiting at the top right. The top end of the wavy line is double-lined.

$$\begin{array}{c}
\text{Diagram 9} = \text{Diagram 10} + \left(\text{Diagram 11} - \text{Diagram 12} \right) \\
\text{(c)}
\end{array}$$

Diagram 9: A vertical oval between two horizontal lines. A wavy line enters from the bottom left, goes up and around the oval, and exits at the top right. The top end of the wavy line is double-lined.

Diagram 10: A vertical oval between two horizontal lines. A wavy line enters from the bottom left, goes up and around the oval, and exits at the top right. The bottom end of the wavy line is double-lined.

Diagram 11: Similar to Diagram 9, but the wavy line enters from the bottom left, goes up and around the oval, and exits at the top right. The top end of the wavy line is double-lined.

Diagram 12: Similar to Diagram 9, but the wavy line enters from the bottom left, goes up and around the oval, and exits at the top right. The bottom end of the wavy line is double-lined.

$$\left(1 + \frac{\text{Diagram 13} - \text{Diagram 14}}{\text{Diagram 15}} \right) \otimes \left(\text{Diagram 16} + \text{Diagram 17} \right)$$

Diagram 13: A vertical oval between two horizontal lines. A wavy line enters from the bottom left, goes up and around the oval, and exits at the top right. The top end of the wavy line is double-lined.

Diagram 14: A vertical oval between two horizontal lines. A wavy line enters from the bottom left, goes up and around the oval, and exits at the top right. The bottom end of the wavy line is double-lined.

Diagram 15: A vertical oval between two horizontal lines.

Diagram 16: A vertical oval between two horizontal lines.

Diagram 17: A vertical oval between two horizontal lines. A wavy line enters from the bottom left, goes up and around the oval, and exits at the top right. The top end of the wavy line is double-lined.

Fig. 1

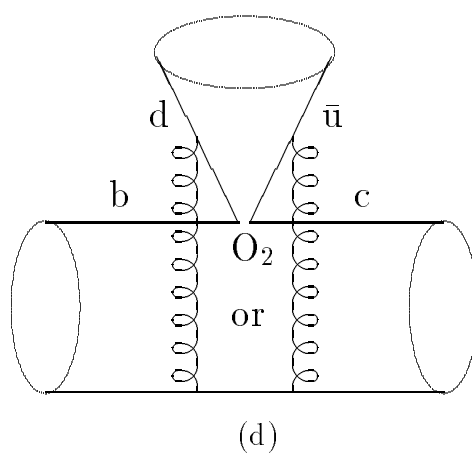
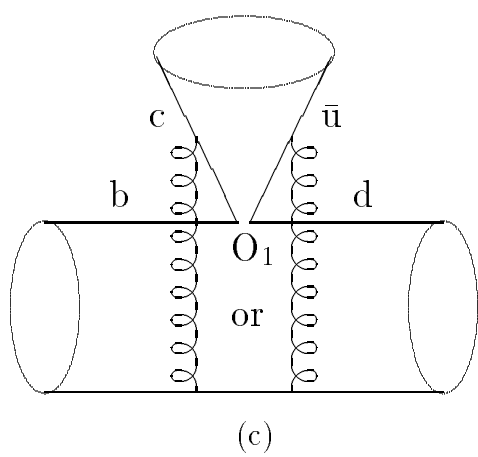
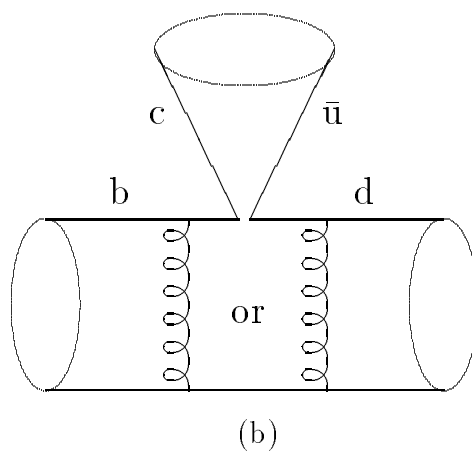
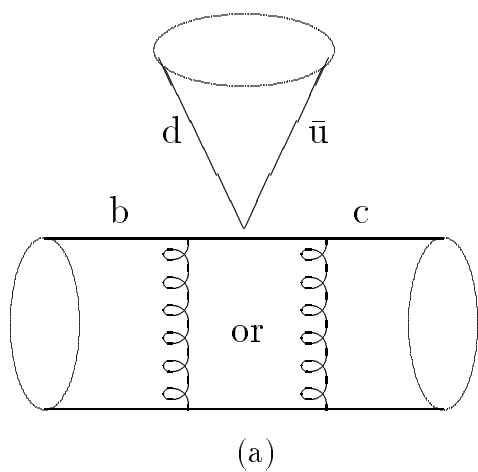


Fig. 2